Review of Scientific Instruments ARTICLE pubs.aip.org/aip/rsi

Cryogenic vacuum valve with actuation times down to 50 ms

Cite as: Rev. Sci. Instrum. 94, 113202 (2023); doi: 10.1063/5.0158043
Submitted: 14 May 2023 • Accepted: 29 October 2023 •
Published Online: 17 November 2023

J. W. Klimes,[1,2,3,a] Kanika,[1,2] A. Krishnan,[1,4] B. Reich,[1,2] K. K. Anjum,[1,5] P. Baus,[4] G. Birkl,[4,6] W. Quint,[1,2] W. Schott,[7] and M. Vogel[1]

AFFILIATIONS

[1] GSI Helmholtzzentrum für Schwerionenforschung, 64291 Darmstadt, Germany
[2] Universität Heidelberg, Grabengasse 1, 69117 Heidelberg, Germany
[3] Max-Planck-Institut für Kernphysik, Saupfercheckweg 1, 69117 Heidelberg, Germany
[4] Technische Universität Darmstadt, Institut für Angewandte Physik, Schlossgartenstraße 7, 64289 Darmstadt, Germany
[5] Friedrich-Schiller-Universität Jena, Max-Wien-Platz 1, 07743 Jena, Germany
[6] Helmholtz Forschungsakademie Hessen für FAIR (HFHF), Campus Darmstadt, Schlossgartenstraße 2, 64289 Darmstadt, Germany
[7] TUM School of Natural Sciences, Technische Universität München, James-Franck-Str. 1, 85748 Garching, Germany

[a] **Author to whom correspondence should be addressed:** j.klimes@gsi.de

ABSTRACT

We have conceived, built, and operated a cryogenic vacuum valve with opening and closing times as short as 50 ms that can be used in strong magnetic fields and across a broad range of duty cycles. It is used to seal a cryogenic Penning trap at liquid-helium temperature for long-term storage of highly charged ions in a vacuum better than 10^{-15} hPa from a room-temperature ion beamline at vacuum conditions around 10^{-9} hPa. It will significantly improve any experiment where a volume at the most extreme vacuum conditions must be temporarily connected to a less demanding vacuum during repeated experimental cycles. We describe the design of this valve and show measurements that characterize its main features.

I. INTRODUCTION

Cryogenic particle traps have emerged as the foremost technology at the precision frontier for experiments in the regime of lowest kinetic energy, in particular enabling fundamental physics studies with exotic matter particles, such as anti-protons and highly charged ions, essentially at rest.[1–6] Highly charged ions provide unprecedented natural laboratories for measurements in the highest electromagnetic fields close to the Schwinger limit,[7] which are currently unavailable at even the strongest high-intensity laser facilities.[8,9] Precision measurements of electromagnetic interactions in such strong fields provide the most stringent tests of quantum electrodynamics in bound states[3,10–15] as well as the properties of the binding nuclei and models of their dielectric shielding.[5,16–18] Such kinds of measurements are currently only possible at this precision with the injection, storage, and cooling of externally produced particles into the well-controlled environment provided by particle traps such as Penning traps.[4] These are typically embedded in a cryogenic surrounding at close to liquid-helium temperature to facilitate the use of low-noise electronics and superconducting equipment, as well as particle cooling and cryo-pumping of the trap vacuum to enable long-term confinement.

Atomic ions in high charge states have limited lifetimes while trapped due to the overwhelming probability of electron capture interactions with residual gas.[19–21] Long-term study of heavy highly charged ions (and likewise of anti-particles such as anti-protons[1]) requires the most extreme vacuum conditions, generally better than 10^{-15} hPa, that are only possible with cryogenic pumping of the residual gases at close to liquid-helium temperature and in excellent sealing conditions.

Given that the creation of such exotic matter requires the use of large accelerators[22,23] or electron beam ion trap (EBIT) facilities,[24] injection into the experimental environment via a beamline necessitates the use of valves that isolate the cryogenic and vacuum conditions of the experiment from the injection beamlines. Such valves need to operate in the usually confined space of cryogenic setups and are faced with the complication that conventional motors and actuators do not work in the strong magnetic fields and cryogenic conditions of such experiments.

Several successful solutions to this problem exist, which are either manually operated[6,25] or utilize slowly rotating devices inside the Penning trap's magnetic field,[26–28] resulting in comparatively long opening and closing times, generally of some minutes. After injection, the trap chamber is hermetically sealed to preserve the experimental conditions until another injection is required, ideally for several days or weeks. In the ARTEMIS experiment using laser-microwave double-resonance spectroscopy,[13,14,29] much shorter and more flexible cycles are required for laser irradiation, thus necessitating a different design choice.

The present solution uses fast and powerful magnetic actuators at room temperature and located outside the strong magnetic field of the trap to drive a thin-walled steel tube. This opens and closes a cryogenic shutter close to the trap inside the magnetic field while maintaining a small heat load on the cryogenic part of the setup.

We show the design of the fast-opening cryogenic valve, including the effects of introducing the thermal connection as well as the resulting conditions of trapped ions after installation of the valve. The stored ions are monitored non-destructively for several days and act as a probe of the residual gas pressure below 2×10^{-15} hPa. The observed opening and closing times of the valve extend the required thermal cycling time of the experiment by about five orders of magnitude.

II. VACUUM REQUIREMENTS

To illustrate the need for an effective separation of the trap vacuum from the beamline vacuum, we look at the expected lifetime of a desired ion charge state as a function of the residual gas pressure. From the electron capture cross section of an atomic ion, according to Müller and Salzborn,[19] it becomes clear that the charge state $\hat{q} = q/e$ of an atomic ion enters the cross section roughly like $\hat{q}^{6/5}$. Hence, the expected lifetime of an ion such as U^{91+} is smaller than that of U^{1+} by a factor of about $91^{6/5} \approx 225$. For the same lifetime to be achieved, the vacuum must thus be improved by that factor. Figure 1 shows the expected charge-state lifetimes[4] of trapped uranium ions for $\hat{q} = 91$ and $\hat{q} = 1$ as a function of the residual He gas pressure across the HV (high vacuum), UHV (ultra-high vacuum), and XHV (extreme-high vacuum) regimes (i.e., at pressures above 10^{-9} hPa, between 10^{-9} and 10^{-12} hPa, and below 10^{-12} hPa, respectively). Precision Penning trap experiments, such as the one presently considered, require stable trapping conditions and the absence of ion-gas reactions for hours, days, or longer. Hence, XHV vacua of 10^{-15} hPa and better are desired, which is possible only by effective separation of the cryo-vacuum of the trap from a room-temperature UHV beamline vacuum of typically 10^{-9} to 10^{-10} hPa.

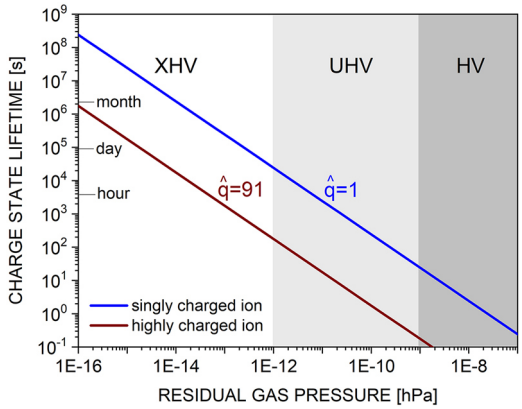

FIG. 1. Expected charge-state lifetimes of trapped uranium ions for charge states $\hat{q} = 91$ and $\hat{q} = 1$ as a function of the residual He gas pressure across the HV, UHV, and XHV vacuum regimes.

III. CRYOGENIC VACUUM

For a better understanding of the valve design, in Sec. IV A, we will briefly discuss the principles of vacua in cryogenic surroundings. Of the numerous techniques used to create vacua, cryo-pumping at close to liquid-helium temperatures is the one that potentially reaches the lowest residual gas pressures. Given that the chamber has been pre-evacuated and the influx of new gas is low, the amount of gas that freezes to the walls of the chamber is sufficiently small. Otherwise, the cryogenic pumping effect is diminished, and the surface may become non-conductive, which is undesirable in traps for charged particles.

Cryogenic vacuum is based on the *cryosorption* effect, by which residual gas atoms in a cryogenic environment are too cold to overcome the molecular bonds between the gas atom and the cryogenic surfaces. A vacuum chamber in the UHV range can initially be pumped well into the XHV range below 10^{-12} hPa by this effect. However, as a monolayer of adsorbed atoms forms on the cryogenic surfaces, the density of atoms in the gas phase will slowly begin to rise, as has been observed in cryogenic Penning traps with a relatively high gas influx.[25] This is depicted in Fig. 2, which is divided into *cryosorption* on the left and relatively weaker *cryocondensation* on the right.[30] When saturation occurs, cryocondensation limits the vacuum pressure to the vapor pressure of the residual gas species, usually H, H_2, and He. At the boiling point of liquid He, the saturated vapor pressure of H_2 is more than 10^{-7} hPa.

In chambers without hermetic seals, the gas atoms that form this layer come predominantly from the opening to the relatively poorer vacuum regions at room temperature, where hydrogen gas slowly permeates the steel walls of the vacuum chamber. The molecular flux in these regions is as high as 10^{11} cm^{-2} s^{-1}. This can be suppressed by using a small aperture of radius r at the end of a long, uniformly cold tube of length l, which limits the ballistic trajectories for gas molecules to enter the cryogenic region. The suppression factor κ can be found from purely geometrical arguments to be

$$\kappa \approx \frac{1}{4}\left(\frac{r}{l}\right)^2. \quad (1)$$

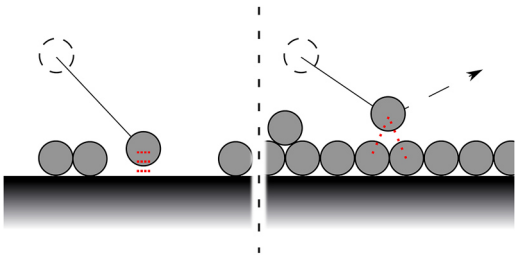

FIG. 2. Drawing of the cryo-pumping effect. Left: Before monolayer formation, incoming gas molecules interact strongly with the cryogenic surface directly and are bound to it. Right: After monolayer formation, gas molecules interact weakly with the molecules already bound to the surface and have an increased probability of scattering back into the gas volume.

For an aperture with a diameter of a few millimeters that is located about a meter from the room temperature region, this suppression is initially on the order of $\kappa \approx 10^{-6}$, leading to monolayer formation times of more than one hundred years. However, the interior volume of such a tube is also susceptible to saturation on the order of days, depending on its inner diameter. Therefore, this suppression is reduced to the relative molecular fluence area of the aperture and the surface area of the cryogenic region. The situation can only be alleviated by improving the room temperature vacuum or introducing a sealing mechanism.

IV. SETUP

The present valve separates our experimental setup, the AsymmetRic Trap for measurement of Electron Magnetic moments in IonS (ARTEMIS) at GSI, from the low-energy beamline[31] for injection of highly charged ions from offline ion sources or from the HITRAP facility.[22,23] ARTEMIS is a cryogenic precision Penning trap for measuring the magnetic moments of electrons and nuclei in highly charged systems[13] such as, e.g., Pb^{81+}, Bi^{82+}, and U^{91+}. It utilizes the laser-microwave double-resonance spectroscopy technique for the determination of magnetic moments by shifts of the (hyper)fine emissions due to induced spin flips with microwave radiation.[13,14] ARTEMIS uses the novel design of the fast-opening cryogenic valve to enable spectroscopy of trapped heavy highly charged ions by opening the trap chamber for only tens of milliseconds. This allows repeated ion injection and irradiation by spectroscopy lasers with a direct line of sight to the trapped ions without compromising the excellent experimental conditions inside the trap region.

In contrast to other implementations of cryogenic valves in Penning traps, the ARTEMIS valve uses the mechanically actuated motion of the shutter to drive opening and closing times as low as 50 ms. The main benefit of this implementation is that, compared to manually[6,25] or electrically actuated motion,[26–28] significantly shorter opening times and arbitrary sequences of opening and closing are possible; however, the main challenge is the introduction of the driving components, which act as a thermal bridge into the cryogenic region.

A. Mechanical design

Here, a detailed description of the fast-opening cryogenic valve design is presented. A complete sectional drawing is shown in Fig. 3 together with a photo of its position mounted directly below the vertical-bore superconducting magnet of ARTEMIS that contains the trap.

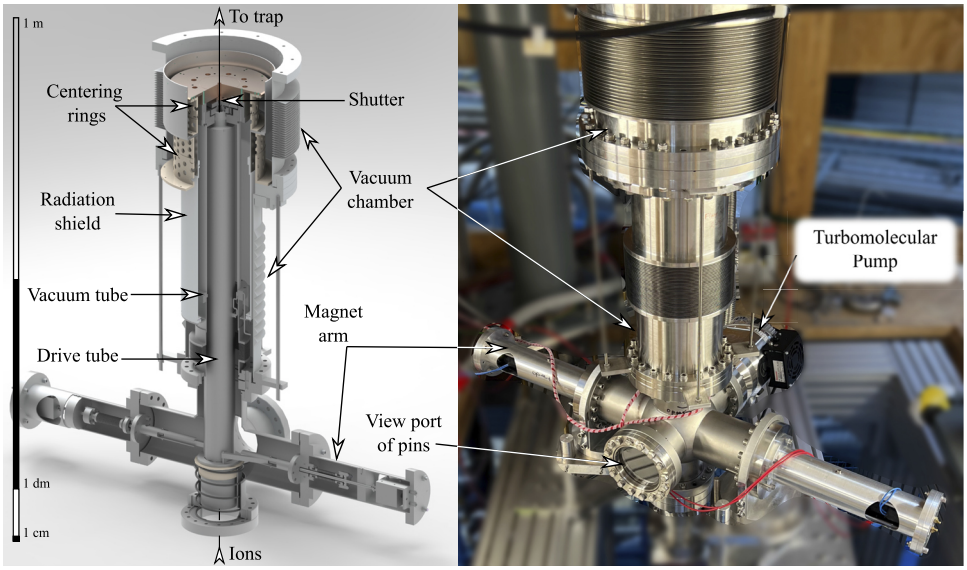

FIG. 3. Left: Sectional drawing of the complete cryo-valve assembly with several key components labeled. Right: Corresponding photograph of the cryo-valve assembled below the ARTEMIS superconducting magnet.

The present valve uses a planar oxygen-free high conductivity (OFHC) copper shutter at the bottom of the cryogenic trap chamber to form a nearly hermetic seal when compressed flush against the valve aperture. All other components in the trap chamber and shutter housing are sealed with compressed indium wire. The shutter is connected to a drive tube such that rotation of the drive tube moves the shutter into or out of the path of the ion/laser beam. This motion is represented in Fig. 4. After saturation of the drive tube, the time averaged leak rate through the shutter due to routine opening is estimated to be on the order of 10^{-14} mbar l s^{-1} and more than an order of magnitude better when the valve is closed. This is achieved by presenting a sufficiently small area for molecular flux around the shutter. The gap between the copper components of the shutter is on the order of tens of micrometers and is minimized by a compressing spring at the bottom of the drive tube at 130 to 160 N.

The drive tube is a 710 mm long stainless steel tube with an inner diameter of 60.8 mm and a thickness of only 0.3 mm. The drive tube is rotated by pulling on pins on the eccentric of the tube with arms ending in solenoid magnets. The length of the drive tube both insulates the cryogenic region and places the driving solenoids in a region of lower magnetic field strength, ~0.5 mT. The housing of the shutter is connected from below to another thin *vacuum tube* with an inner diameter of 85 mm, a thickness of 0.25 mm, and a length of 352 mm. Below the vacuum tube, there is an edge-welded bellows, which allows the vacuum and drive tube to be raised or lowered relative to the outer vacuum chamber of the valve. These thin stainless steel tubes act as thermal insulators between the cryogenic region at the top and the room-temperature region at the bottom.

The thin vacuum tube separates the vacuum region of the bore of the superconducting magnet from the vacuum of the injection beamline below the valve. This tube can sustain a pressure differential of about 300 hPa before deforming. To ensure that the pressure difference between these two regions never exceeds this value, the chambers are coupled by their backing lines for their respective turbomolecular pumps (TMP), one located at the top of the magnet bore and one at the crosspiece of the valve. This setup is shown diagrammatically in Fig. 5. During initial evacuation or at the end of venting, the residual air is in the continuous flow regime, and the pressure naturally equalizes between the two vacuum sections, limited only by the conductance of the chambers and connecting hoses. Once free molecular flow is reached, the separate turbomolecular pumps allow the beamline to reach pressures of 10^{-9} hPa or better without being limited by the relatively high pressure in the magnet bore of 10^{-7} hPa.

The connection between the top of the valve and the trap chamber, as well as the upper portion of the vacuum tube, is surrounded by an aluminum radiation shield, which is connected to the radiation shield of the trap chamber by copper strands, which is in turn mounted to the 40 K stage of a pulse tube cryocooler. Additional copper strands are connected between the bottom edge of the radiation shield and the vacuum tube, as well as between the vacuum tube and the middle of the drive tube. Multilayer insulation foil is

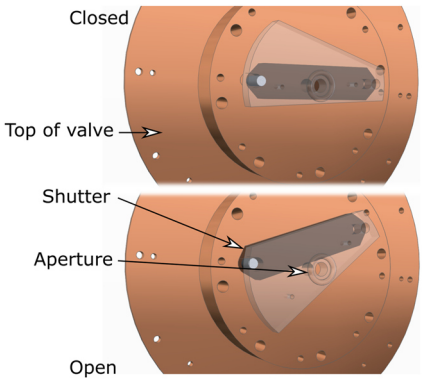

FIG. 4. Schematic of the cryo-valve shutter mechanism. The rendered partially transparent part is the end of the stainless steel drive tube. Top: Closed state with the shutter blocking the aperture. Bottom: Open state after the drive tube is turned, rotating one end of the shutter while the opposite end is fixed to a radial path. Minimal opening of the 5 mm aperture is achieved by a 43.5° rotation of the drive tube.

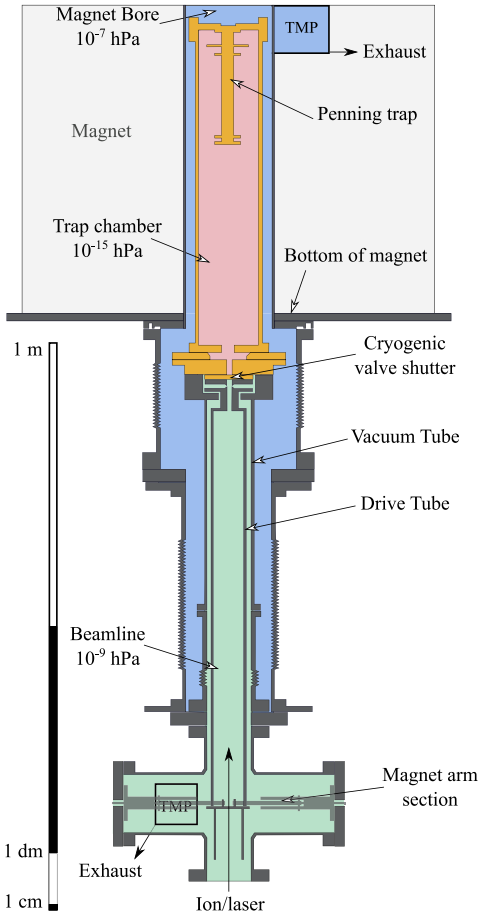

FIG. 5. Sectional schematic of the valve with the three different vacuum regions indicated by the three shaded areas. Blue: isolation vacuum of the magnet bore. Green: beamline vacuum. Pink: trap vacuum. The trap chamber is initially evacuated through the valve to maintain UHV pressure, and the cryo-pumping effect maintains XHV pressures after cooling. TMP indicates the mounting positions of the two turbomolecular pumps.

wrapped around each of the layers of the valve to minimize radiative heat transfer between them as well as cover the small gap between the shields of the trap and the valve.[32]

The weight of the trap chamber, shutter, and vacuum and drive tubes of the valve are supported by rings of polyether ether ketone (PEEK), which is a commercial vacuum-compatible plastic thermal insulator. These rings also center the position of the trap electrodes within the most homogeneous region of the magnetic field.

The magnet arms are mounted at a sufficient distance from the superconducting magnet that they can be operated with fast pulses from a control box. They drive the rotation of the valve, and their stroke length is limited to a minimal path. The control box uses two 1 mF capacitors to generate the large-current pulses that drive the magnets. The timing of the pulses—their width, duration of the pause between pulses, and the delay following the box trigger—can be freely programmed between 10 and 1000 ms.

B. Heat loads of the fast-opening cryogenic valve

The design with mechanically actuated motion necessitates mechanically connected components, which results in an increased thermal load on the cryogenic components of the valve as well as the trap chamber by conductance. This heat is dissipated at cryogenic temperatures by a Sumitomo RP-082B pulse tube cryocooler, which is rated for 1 W cooling power at 4.2 K on its second stage and 40 W at 40 K on its first stage. The thermal conductance is limited by the choice of materials and the minimization of their cross-sectional area. Additionally, a significant amount of heat transfer can be shunted from the second stage of the cryocooler to the first by thermal coupling of components at specific points along lengths with high temperature gradients. An example is shown in Fig. 6,

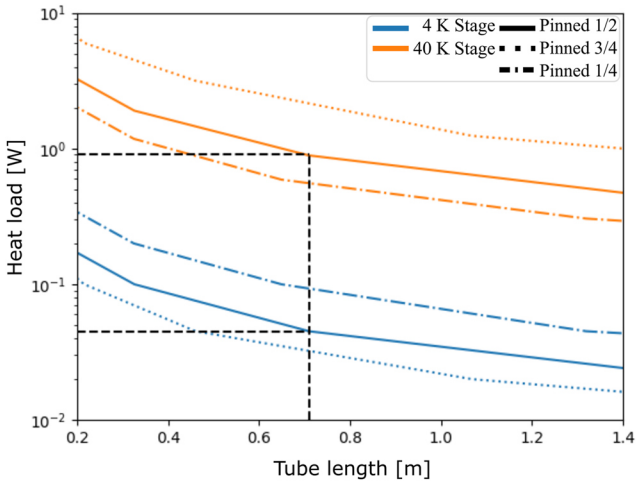

FIG. 6. Simulated heat loads for various lengths of drive tubes, with the tube coupled to the 40 K radiation shield at the midpoint. The solid blue and orange curves show the heat delivered to the 4 and 40 K stages of the cold head, respectively. The dotted and dashed–dotted curves show the heat load when moving the coupling to the radiation shield to 1/4 or 3/4 of the tube length as measured from the cold end. Finally, the black dashed lines show the loads in the final design of the present valve. The presented values were determined by a finite difference model in Python®.

which is the theoretical heat load of drive tubes of various lengths that are cooled to 4 K at one end, coupled to the first stage of the cryocooler at 1/4, 1/2, and 3/4 of their length as measured from the cold end, and held at room temperature at the opposite end. The black lines indicate the final design length of the drive tube used in the cryogenic valve at 45 mW to the second stage and 890 mW to the first.

Similarly, the vacuum tube is estimated to deliver 53 mW to the second stage and less than 2 W to the first stage, depending on the exact thickness of the edge-welded bellows of its lower section. The estimation of the heat delivered through the PEEK support rings is more complicated due to their geometry. A finite element simulation in COMSOL® of the 3D temperature gradient was used to determine the area of isotherms in the design with the holes. This was then used to set expected heat loads of 8 mW for the 4 K stage and 760 mW for the 40 K stage. These values represent a reduction of 53% and 42%, respectively, compared to the same shape with unbroken radial symmetry.

In addition, the introduction of the valve increases the length of the cryogenic region by more than 50% compared to the setup before the installation of the valve. This significantly increases the effective area for radiative heat transfer. For concentric cylinders of low emissivity and nearly equal radius at 40 and 4 K, this effect is about 5 mW/m^2. This can be further reduced by the application of multilayer insulation foil. The upper estimate of the radiative heat transfer from radiation shields of uniform temperature to the cryogenic components is about 220 mW.

As several components of different temperatures have similar sizes, the possibility of incidental contact and unaccounted thermal pathways must be considered. Although the exact load introduced by such contact cannot be quantitatively modeled, the known loads account for only a portion of the heat budget for the given temperatures. Moreover, the thermal conductivity of the materials in question is increasing as a function of their temperature, which causes positive feedback on the conductive load.

Finally, the aluminum radiation shields could sustain a significant thermal gradient along their more than 2 m total length, given the significant heat radiated from their room temperature surroundings. The observed final temperatures and associated heat loads indicate a temperature gradient of up to 63 K, which would in turn increase the heat radiated onto the lowermost cryogenic components.

V. EXPERIMENTAL RESULTS

To date, the present valve has been used in two experimental runs. The operational goals of the valve are demonstrated by the successful and reliable opening and closing of the valve and a pressure better than the current experimental requirements. The cryogenic valve enables fast, repeated opening and closing of the trap region without compromising the cryogenic and vacuum conditions within the trap. The opening and closing of the valve during operation are monitored through a window on the cross of the valve. The temperature of the trap chamber and radiation shields is monitored by a pair of calibrated carbon ceramic temperature sensors with mK accuracy. However, fluctuations due to daily cycles as well as environmental changes cause a standard deviation of the temperature distribution of 0.8 K throughout a three to four month run. The

average measured temperature of the trap chamber was 8.792(75) and 11.0(8) K for the first two runs with the valve, sufficient for efficient cryo-pumping of residual gases. These temperatures indicate a total increase in the heat load of 3 W, which is consistent with a radiation dominant heating mode.

A. Vacuum measurements

The pressure in the room-temperature UHV beamline below the valve is measured directly with an inverted magnetron gauge and has remained within the expected range required for the estimated gas density and corresponding molecular flux throughout the operation. In contrast, vacua well in the XHV regime cannot be measured directly but can be inferred from measurements of the lifetime of stored particles with regard to electron capture or other reactions with the residual gas, provided that the respective reaction cross section is known sufficiently well.[4] Presently, the residual gas pressure in the trap chamber with the shutter closed was determined by monitoring a trapped ensemble of ions over a period of several days. A non-destructive monitoring technique based on image currents induced by the ions' motions is used to resolve the contents of the trap according to their charge-to-mass ratios.[4] The power density within the peaks of such a spectrum is proportional to the respective ion numbers.[33] The spectrum of such a measurement after electron impact ionization[34] of the adsorbed residual gas with a long breeding time is shown at the top of Fig. 7. It contains the expected main constituents of residual gas in various charge states.

For better control of systematic effects, the ion number for the pressure determination was kept low using an electron beam with an intensity of just 200 nAs for ionization. The ion population of such a *cold* creation is stochastic, and for this run, it consisted of primarily N^{4+} with a small admixture of other ion species. The ensemble was then reduced to purely N^{4+} by application of the SWIFT technique[35,36] to ensure no other contaminant species were present. The middle spectrum of Fig. 7 shows the initial scan of the trap following creation as well as the spectrum after SWIFT. This ion cloud was then resistively cooled as it was monitored until it was nearly in thermal equilibrium with the trap environment.[33] Afterward, a detailed scan of the frequency distribution of the trapped ions was measured using the same technique and repeated every couple of hours. The trapped ions were tuned out of resonance with the detection system between scans so that they were completely isolated from the environment. A Lorentzian curve was then fit to the result of each scan to extract the amplitude, center frequency, and width of the ion signal. The final spectrum of Fig. 7 shows the result of a single scan during the over 40-h storage time and the corresponding fit to the data.

Scans within the expected range of N^{3+} ions indicated no significant population above the noise floor. This observation is used to determine an upper limit on the rate of N^{3+} ion creation by charge exchange interactions with the residual gas. Using the measured signal power of N^{4+} and this upper limit of N^{3+}, the ratio of N^{3+} to N^{4+} ions is given by

$$\frac{N_{N^{3+}}}{N_{N^{4+}}} = \frac{4\Sigma_{N_{N^{3+}}}}{3\Sigma_{N_{N^{4+}}}} < \frac{4}{3}\frac{s}{\Sigma_{N_{N^{4+}}}}, \tag{2}$$

where N_i indicates the population of species i, s is the standard deviation of the noise distribution, and Σ_i is the power of the ion signal of species i. Figure 8 shows the histograms of the measured power in the band for scans about the two frequency regions for N^{4+} and N^{3+} ions, as indicated by the colored coordinated regions in the middle of Fig. 7. The upper limit of this ratio is 0.0058 for the given distribution of noise. The probability of a single N^{4+} ion undergoing charge exchange in time Δt is given by

$$\mathcal{P} = n\sigma\langle v\rangle\Delta t = \frac{N_{N^{3+}}}{N_{N^{4+}}}, \tag{3}$$

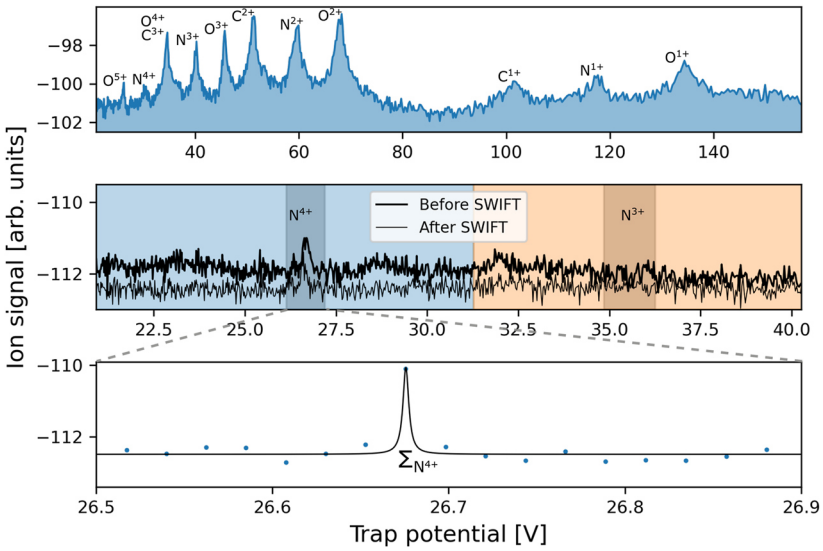

FIG. 7. Measured charge-to-mass spectrum of trapped ions created from electron impact ionization of adsorbed residual gas inside the trap: *hot* creation (top) and *cold* creation (middle). The blue and orange highlighted regions indicate a broad range of the theoretical positions of N^{4+} and N^{3+}, which were used for pressure determination. A detailed view of the N^{4+} peak near thermal equilibrium shows the fit and extracted amplitude (bottom).

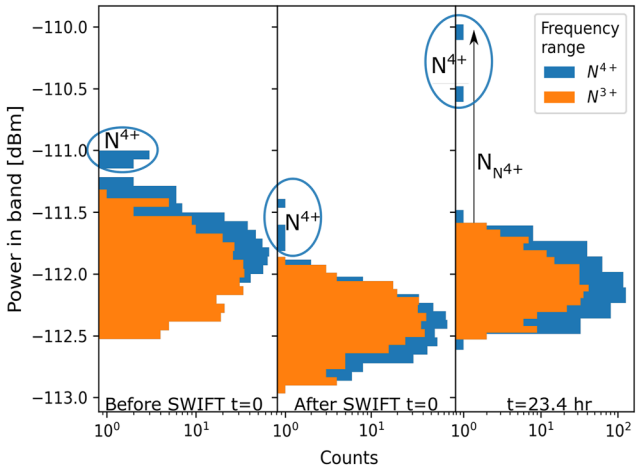

FIG. 8. Histograms of the spectra within the shaded regions shown in the middle frame of Fig. 7. The top signal at about −110 dBm in the right histogram indicates the population of N^{4+} ions after about one day, and the distribution of the noise at lower power is used to quantitatively estimate an upper limit for the residual N^{3+} population.

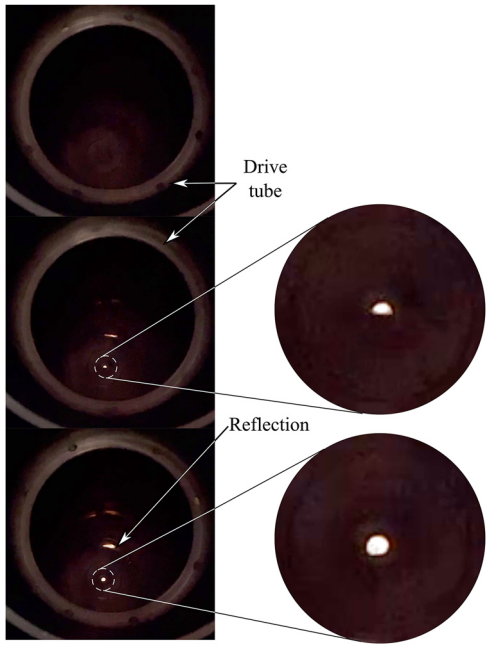

FIG. 9. Three successive frames showing the position of the shutter during an opening pulse. The frame resolution is 33 ms. The first frame shows a completely closed shutter, followed by a partially open shutter, and then a fully open shutter. Inset images show a zoomed-in view of the aperture.

where n is the number density of residual gas molecules, σ is the single-charge-exchange cross section with the background gas, and $\langle v \rangle$ is the average velocity of the interaction. The upper pressure limit P is extracted from the residual gas density by treating the gas as ideal,

$$P = nRT = \frac{RT}{\sigma \langle v \rangle \Delta t} \frac{N_{N^{3+}}}{N_{N^{4+}}}, \tag{4}$$

where $R = 8.314$ J K^{-1} mol^{-1} is the gas constant and T is the temperature. Using the cross section predicted by Müller and Salzborn[19] for a hydrogen gas background of 5.59×10^{-15} cm^2 and the recorded temperature during the measurement time, the pressure in the trap with the shutter closed is found to be below 1.4×10^{-15} hPa.

B. Shutter opening time measurements

The opening and closing times of the shutter were determined by monitoring its position with a camera (frame resolution of 33 ms) without the trap chamber attached. This represents a reasonable measure of the upper limit on the opening time until fast timing data can be collected using a laser beam that is chopped by the shutter and a photodiode for fast detection. To account for the magnetoresistance of the magnet arms and the eddy current breaking of the rotating conductive parts, the valve was placed in the position below the superconducting magnet corresponding to an experimental run. In this position, the magnetic field strength at the shutter position is about 0.6 T. Figure 9 shows the images of the successive frames of the video immediately following the opening pulse.

Application of an opening pulse with a duration of 40 ms or less results in no motion of the shutter, while a duration of 50 ms or more allows an individual frame with a partially open shutter to be observed. As there was no synchronization of the opening pulse and the camera frames, an upper limit on the opening time can be placed at twice the frame resolution of the camera, or 66 ms. This is sufficiently fast to push the monolayer saturation time above 10^5 opening cycles. A qualitative limit on the duty cycle of the valve is set by the charging rate of the control box capacitors, which deliver reduced power to the opening magnets for triggers separated by less than about 1 s. This is well below the anticipated injection cycle for heavy, highly charged ions of about 90 s.[22,23]

VI. CONCLUSION

We have presented the principles, design, and operational results for a novel cryogenic isolation valve with sub-second opening times. It utilizes the physical adsorption of residual gas molecules at cryogenic temperatures to reduce the pressure well into the extreme-high vacuum (XHV) range as required, e.g., for precision experiments with heavy highly charged ions. It allows repeated opening and closing of a shutter on time scales as short as about 50 ms in strong magnetic fields and liquid-helium temperatures by separating the shutter from its actuators by a rigid drive tube of low thermal conductivity embedded in a suitable vacuum environment. The timing of the operation is arbitrary, with any duty cycle (repetition time) above about 1 s. To achieve opening within around 50 ms, the valve introduces mechanically actuated control of the shutter mechanism and, therefore, increased heat load to the cryogenic region. A detailed simulation of these loads was used to design a valve that could be operated down to temperatures of only a few Kelvin. The experimental upper pressure limit in the trap of about 10^{-15} hPa has been determined by observation of stored ions with no observed charge exchange over a period of days. More stringent limits on both the pressure and ultimate temperature are expected

with upcoming improvements to the valve as well as the detection system of the experiment.

ACKNOWLEDGMENTS

We acknowledge financial support by the Federal Ministry of Education and Research (BMBF) [Grant Nos. 05P21RDFA1 and 05P2021 (ErUM-FSP T05)], by the Helmholtz Forschungsakademie Hessen für FAIR (HFHF), the R&D cooperation agreements between GSI/FAIR, Heidelberg University, and TU Darmstadt, the European Union's Horizon 2020 research and innovation program under the Marie Sklodowska-Curie Grant Agreement No. 721559 "Accelerators Validating Antimatter physics (AVA)," the International Max Planck Research School for Quantum Dynamics (IMPRS-QD), and by the Helmholtz Graduate School for Hadron and Ion Research (HGS-HIRe for FAIR). We further acknowledge the work performed by Peter Hartung and Christian Vogel, whose efforts paved the way for the presented work.

AUTHOR DECLARATIONS

Conflict of Interest

The authors have no conflicts to disclose.

Author Contributions

J. W. Klimes: Data curation (equal); Formal analysis (lead); Investigation (equal); Methodology (equal); Software (equal); Visualization (equal); Writing – original draft (equal); Writing – review & editing (equal). **Kanika**: Data curation (equal); Investigation (equal); Methodology (equal); Software (equal); Writing – review & editing (equal). **A. Krishnan**: Data curation (equal); Investigation (equal); Methodology (equal); Software (supporting); Writing – review & editing (equal). **B. Reich**: Data curation (equal); Investigation (equal); Methodology (equal); Software (equal); Writing – review & editing (equal). **K. K. Anjum**: Investigation (supporting); Methodology (equal); Software (supporting); Writing – review & editing (equal). **P. Baus**: Methodology (equal); Software (equal); Writing – review & editing (equal). **G. Birkl**: Conceptualization (equal); Funding acquisition (equal); Methodology (equal); Project administration (equal); Resources (equal); Supervision (equal); Writing – review & editing (equal). **W. Quint**: Conceptualization (equal); Funding acquisition (equal); Methodology (equal); Project administration (equal); Resources (equal); Supervision (equal); Writing – review & editing (equal). **W. Schott**: Conceptualization (lead); Supervision (equal); Writing – review & editing (equal). **M. Vogel**: Conceptualization (equal); Funding acquisition (equal); Methodology (equal); Project administration (equal); Resources (equal); Supervision (equal); Writing – original draft (equal); Writing – review & editing (equal).

DATA AVAILABILITY

The data that support the findings of this study are available from the corresponding author upon reasonable request.

REFERENCES

[1] C. Smorra, K. Blaum, L. Bojtar, M. Borchert, K. A. Franke, T. Higuchi, N. Leefer, H. Nagahama, Y. Matsuda, A. Mooser, M. Niemann, C. Ospelkaus, W. Quint, G. Schneider, S. Sellner, T. Tanaka, S. Van Gorp, J. Walz, Y. Yamazaki, and S. Ulmer, Eur. Phys. J. Spec. Top. **224**, 3055 (2015).
[2] W. Quint and M. Vogel, *Fundamental Physics in Particle Traps* (Springer, 2014).
[3] S. Sturm, M. Vogel, F. Köhler-Langes, W. Quint, K. Blaum, and G. Werth, Atoms **5**, 4 (2017).
[4] M. Vogel, *Particle Confinement in Penning Traps: An Introduction* (Springer, 2018).
[5] H. F. Beyer and V. P. Shevelko, *Introduction to the Physics of Highly Charged Ions* (CRC Press, 2002).
[6] S. Sturm, I. Arapoglou, A. Egl, M. Höcker, S. Kraemer, T. Sailer, B. Tu, A. Weigel, R. Wolf, J. C. López-Urrutia, and K. Blaum, Eur. Phys. J. Spec. Top. **227**, 1425 (2019).
[7] J. Schwinger, Phys. Rev. **82**, 664 (1951).
[8] G. Soff, I. Bednyakov, T. Beier, F. Erler, I. Goidenko, U. Jentschura, L. Labzowsky, A. Nefiodov, G. Plunien, R. Schützhold, and S. Zschocke, Hyperfine Interact. **132**, 75 (2001).
[9] S. S. Bulanov, T. Z. Esirkepov, A. G. R. Thomas, J. K. Koga, and S. V. Bulanov, Phys. Rev. Lett. **105**, 220407 (2010).
[10] T. Beier, Phys. Rep. **339**, 79 (2000).
[11] S. Sturm, A. Wagner, M. Kretzschmar, W. Quint, G. Werth, and K. Blaum, Phys. Rev. A **87**, 030501 (2013).
[12] P. Micke, T. Leopold, S. A. King, E. Benkler, L. J. Spieß, L. Schmöger, M. Schwarz, J. R. Crespo López-Urrutia, and P. O. Schmidt, Nature **578**, 60 (2020).
[13] W. Quint, D. L. Moskovkhin, V. Shabaev, and M. Vogel, Phys. Rev. A **78**, 032517 (2008).
[14] D. von Lindenfels, M. Wiesel, D. A. Glazov, A. V. Volotka, M. M. Sokolov, V. M. Shabaev, and G. Plunien *et al.*, Phys. Rev. A **87**, 023412 (2013).
[15] V. M. Shabaev, A. I. Bondarev, D. A. Glazov, M. Y. Kaygorodov, Y. S. Kozhedub, I. A. Maltsev, A. V. Malyshev, R. V. Popov, I. I. Tupitsyn, and N. A. Zubova, Hyperfine Interact. **239**, 60 (2018).
[16] D. L. Moskovkin, N. S. Oreshkina, V. M. Shabaev, T. Beier, G. Plunien, W. Quint, and G. Soff, Phys. Rev. A **70**, 032105 (2004).
[17] V. M. Shabaev, D. A. Glazov, M. B. Shabaeva, V. A. Yerokhin, G. Plunien, and G. Soff, Phys. Rev. A **65**, 062104 (2002).
[18] J. Zatorski, N. S. Oreshkina, C. H. Keitel, and Z. Harman, Phys. Rev. Lett. **108**, 063005 (2012).
[19] A. Müller and E. Salzborn, Phys. Lett. A **62**, 391 (1977).
[20] R. Mann, Z. Phys. D **3**, 85 (1986).
[21] R. E. Olson and A. Salop, Phys. Rev. A **16**, 531 (1977).
[22] H. J. Kluge, T. Beier, K. Blaum, L. Dahl, S. Eliseev, F. Herfurth, B. Hofmann, O. Kester, S. Koszudowski, S. C. Kozhuharov, G. Maero, W. Nörtershäuser, J. Pfister, W. Quint, U. Ratzinger, A. Schempp, R. Schuch, T. Stöhlker, R. C. Thompson, M. Vogel, G. Vorobjev, D. F. A. Winters, and G. Werth, Adv. Quantum Chem. **53**, 83 (2007).
[23] F. Herfurth, Z. Andelkovic, W. Barth, W. Chen, L. Dahl, S. Fedotova, P. Gerhard, M. Kaiser, O. K. Kester, H. J. Kluge, N. Kotovskiy *et al.*, Phys. Scr. **T166**, 014065 (2015).
[24] M. A. Levine, R. E. Marrs, J. R. Henderson, D. A. Knapp, and M. B. Schneider, Phys. Scr. **T22**, 157 (1988).
[25] L. Gruber, J. P. Holder, and D. Schneider, Phys. Scr. **71**, 60 (2005).
[26] P. S. Yesley, "The road to antihydrogen," Ph.D. thesis, Harvard University, 2001.
[27] C. Smorra, S. Gavranovic, D. Popper, S. Ulmer, J. Devlin, Y. Dutheil, B. Latacz, E. Wursten, M. Bohman, M. Borchert, S. Erlewein, V. Grunhofer, M. Wiesinger, K. Blaum, Y. Matsuda, A. Mooser, C. Ospelkaus, W. Quint, J. Walz, and Y. Yamazaki BASE, Technical Design Report of BASE-STEP, Tech. Rep., CERN, Geneva, 2021.
[28] T. Aumann, W. Bartmann, O. Boine-Frankenheim, A. Bouvard, A. Broche, F. Butin, D. Calvet, J. Carbonell, P. Chiggiato, H. De Gersem, R. De Oliveira, T. Dobers, F. Ehm, J. F. Somoza, J. Fischer, M. Fraser, E. Friedrich, A. Frotscher, M. Gomez-Ramos, J.-L. Grenard, A. Hobl, G. Hupin, A. Husson, P. Indelicato, K. Johnston, C. Klink, Y. Kubota, R. Lazauskas, S. Malbrunot-Ettenauer, N. Marsic, W. F. O. Müller, S. Naimi, N. Nakatsuka, R. Necca, D. Neidherr, G. Neyens,

A. Obertelli, Y. Ono, S. Pasinelli, N. Paul, E. C. Pollacco, D. Rossi, H. Scheit, M. Schlaich, A. Schmidt, L. Schweikhard, R. Seki, S. Sels, E. Siesling, T. Uesaka, M. Vilén, M. Wada, F. Wienholtz, S. Wycech, and S. Zacarias, Eur. Phys. J. A **58**, 88 (2022).
[29]M. Vogel, M. S. Ebrahimi, Z. Guo, A. Khodaparast, G. Birkl, and W. Quint, Ann. Phys. **531**, 1800211 (2018).
[30]C. Benvenuti, "Extreme vacua: Achievements and expectations," Phys. Scr. **1988**(T22), (1988).
[31]Z. Andelkovic, F. Herfurth, N. Kotovskiy, K. König, B. Maaß, T. Murböck, D. Neidherr, S. Schmidt, J. Steinmann, M. Vogel, and G. Vorobjev, Nucl. Instrum. Methods Phys. Res., Sect. A **795**, 109 (2015).
[32]B. Baudouy, "Heat transfer and cooling techniques at low temperature," CERN Accelerator School: Course on Superconductivity for Accelerators, edited by R. Bailey, CERN, 2014.
[33]M. S. Ebrahimi, Z. Guo, M. Vogel, M. Wiesel, G. Birkl, and W. Quint, Phys. Rev. A **98**, 023423 (2018).
[34]Kanika, A. Krishnan, J. W. Klimes, B. Reich, K. Anjum, P. Baus, G. Birkl, W. Quint, and M. Vogel, J. Phys. B: At. Mol. Opt. Phys. **56**, 175001 (2023).
[35]S. Guan and A. G. Marshall, Int. J. Mass Spectrom. Ion Processes **157–158**, 5 (1996).
[36]A. G. Marshall, C. L. Hendrickson, and G. S. Jackson, Mass Spectrom. Rev. **17**, 1 (1998).